Tuning the glass-forming ability of metallic glasses through energetic frustration

Yuan-Chao Hu,[1] Jan Schroers,[1] Mark D. Shattuck,[2] and Corey S. O'Hern[1,3,4,*]

[1]*Department of Mechanical Engineering & Materials Science, Yale University, New Haven, Connecticut 06520, USA*
[2]*Benjamin Levich Institute and Physics Department, The City College of New York, New York, New York 10031, USA.*
[3]*Department of Physics, Yale University, New Haven, Connecticut 06520, USA.*
[4]*Department of Applied Physics, Yale University, New Haven, Connecticut 06520, USA.*

(Dated: April 7, 2019)

The design of multi-functional BMGs is limited by the lack of a quantitative understanding of the variables that control the glass-forming ability (GFA) of alloys. Both geometric frustration (e.g. differences in atomic radii) and energetic frustration (e.g. differences in the cohesive energies of the atomic species) contribute to the GFA. We perform molecular dynamics simulations of binary Lennard-Jones mixtures with only energetic frustration. We show that there is little correlation between the heat of mixing and critical cooling rate R_c, below which the system crystallizes, except that $\Delta H_{\rm mix} < 0$. By removing the effects of geometric frustration, we show strong correlations between R_c and the variables $\epsilon_- = (\epsilon_{BB} - \epsilon_{AA})/(\epsilon_{AA} + \epsilon_{BB})$ and $\bar{\epsilon}_{AB} = 2\epsilon_{AB}/(\epsilon_{AA} + \epsilon_{BB})$, where ϵ_{AA} and ϵ_{BB} are the cohesive energies of atoms A and B and ϵ_{AB} is the pair interaction between A and B atoms. We identify a particular f_B-dependent combination of ϵ_- and $\bar{\epsilon}_{AB}$ that collapses the data for R_c over nearly 4 orders of magnitude in cooling rate.

Bulk metallic glasses (BMGs) are amorphous alloys that possess promising structural, mechanical, and functional properties [1–3]. However, a given BMG may not possess multiple desirable properties, such as high elastic strength and biocompatibility in the case of BMGs used in biomedical applications [4]. Thus, *de novo* design of BMGs with multi-functional properties is an important goal. A key impediment to progress is that one cannot currently predict the glass-forming ability (GFA) of a given alloy [5]. The most prominent and widely used features for identifying BMGs were suggested by Inoue in 2000 [6]: 1) BMGs are typically multicomponent systems consisting of three or more elements, 2) the size ratios of the three main constituents differ by more than 12%, and 3) the heat of mixing $\Delta H_{\rm mix}$ among the three main elements is negative. However, there are many examples of metallic glasses that do not obey these rules. First, several binary alloys (such as CuZr) possess GFAs that are comparable to those for multi-component BMGs [7–9]. Also, there are many ternary alloys (e.g. Al, Cu, and V) that have $R_c < 10^6$ K/s, but the diameter ratios among the three elements differ by less than 12% [10]. Further, recent experimental studies have shown that even monoatomic metallic systems can form glasses via rapid cooling [11]. Thus, it is clear that a more quantitative theoretical framework is necessary for predicting the GFA of alloys.

There are two main contributions to the GFA of an alloy, geometric and energetic frustration [12, 13]. Geometric frustration can be achieved in alloys using elements with sufficiently different metallic radii [12, 14, 15], which allows the glass phase to pack more desely, but severely strains the competing crystalline phases. Energetic frustration can be achieved in alloys even with elements of similar sizes, if they possess different cohesive energies and strong interactions between different atomic species. While there have been many computational studies of the variation of R_c with geometric frustration [13, 16, 17], there are few studies that have investigated how energetic frustration in the absence of geometric frustration affects the GFA.

In this Letter, we carry out molecular dynamics simulations of binary Lennard-Jones (LJ) mixtures with atoms of the same size, but different cohesive energies, to understand the critical cooling rate as a function of the degree of energetic frustration. We find several important results: 1) We show that there is little correlation between the GFA and heat of mixing in binary and multicomponent metallic glass formers. 2) Instead, we find that there is a particular combination of the difference in the cohesive energies and the pair interactions among different species in binary alloys that yields the best GFA for each composition. 3) We rationalize these findings for binary LJ systems with the best GFA by considering separation fluctuations and chemical ordering [18] among nearest neighbor atoms.

We focus on binary LJ mixtures in three dimensions with vanishing geometric, but tunable energetic frustration. The pairwise interaction potential is:

$$V(r_{ij}) = 4\epsilon_{ij}\left[\left(\frac{\sigma}{r_{ij}}\right)^{12} - \left(\frac{\sigma}{r_{ij}}\right)^{6}\right], \qquad (1)$$

where σ is the diameter of atoms A and B, r_{ij} is the separation between atoms i and j, ϵ_{AA} and ϵ_{BB} are the cohesive energies of atoms A and B, and ϵ_{AB} is the interaction energy between A and B. The potential is truncated and shifted at $r_{ij} = 2.5\sigma$, and the total potential energy is $V = \sum_{i>j} V(r_{ij})$. We consider $N = N_A + N_B = 2000$ atoms with equal mass $m_A = m_B$ in a cubic box and

periodic boundary conditions in all directions. Length, energy, pressure, and time scales will be reported in units of σ, ϵ_{AA}, ϵ/σ_{AA}^3, and $\sqrt{m_A\sigma/\epsilon_{AA}}$.

We first equilibrate each system with a fraction of B atoms, $f_B = N_B/N$, and combinations of $\epsilon_{BB}/\epsilon_{AA}$ and $\epsilon_{AB}/\epsilon_{AA}$ at high temperature $T = 5.0$ (using a Nose-Hoover thermostat [19, 20]) and then quench them to low temperature $T = 0.01$ as a function of cooling rate R. The thermal quenches are performed at fixed pressure $P_0 = 10$ to avoid cavitation [21]. We find that the particular value of P_0 does not strongly affect the GFA in systems that do not cavitate over the range $10^{-2} < P_0 < 10$. (See Supplemental Material.)

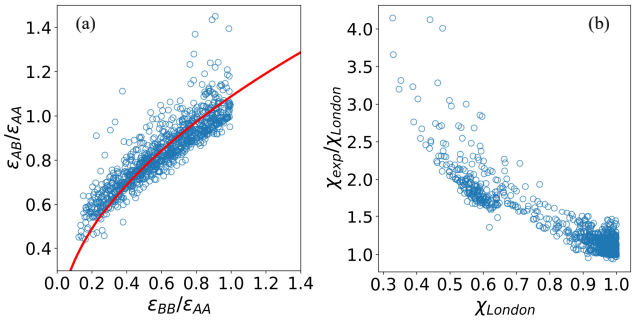

FIG. 1. (a) The interaction energy ϵ_{AB} (normalized by ϵ_{AA}) from the pairwise heat of mixing ΔH_p plotted versus the cohesive energy ratio $\epsilon_{BB}/\epsilon_{AA}$ for 990 binary alloys involving 45 elements found in metallic glasses [22, 23]. We chose element A, such that $\epsilon_{AA} > \epsilon_{BB}$. The solid line obeys $\epsilon_{AB} = c\sqrt{\epsilon_{BB}\epsilon_{AA}}$ with $c = 1.09$. (b) The ratio of $\chi_{\rm exp} = \epsilon_{AB}/\sqrt{\epsilon_{AA}\epsilon_{BB}}$ to the London expression, $\chi_{\rm London}$ in Eq. 2, plotted versus $\chi_{\rm London}$ for the same data in (a).

To understand the relevant range of parameter space for the cohesive energies, ϵ_{AA} and ϵ_{BB}, and interaction energy ϵ_{AB}, we cataloged these values for 990 binary alloys involving 45 elements that occur in metallic glasses. For this analysis, we chose element A such that $\epsilon_{AA} > \epsilon_{BB}$ and used the pairwise definition of the heat of mixing, $\Delta H_p(i,j) = (\epsilon_{ii} + \epsilon_{jj})/2 - \epsilon_{ij}$, to calculate ϵ_{AB} [24]. Values for ϵ_{AA}, ϵ_{BB}, and ΔH_p were obtained from experimental data [22, 23]. In Fig. 1 (a), we show that binary alloys exist over a narrow range of parameters, $0.5 \lesssim \epsilon_{AB}/\epsilon_{AA} \lesssim 1.4$ and $0.1 \lesssim \epsilon_{BB}/\epsilon_{AA} < 1$. In contrast, these energetic parameters can exist over a wider range in ionic liquids and molten salts [25, 26]. Albeit with scatter, the experimental data scales as $\epsilon_{AB} \propto \sqrt{\epsilon_{AA}\epsilon_{BB}}$, which is similar to the London mixing rule $\epsilon_{AB} = \chi_{\rm London}\sqrt{\epsilon_{AA}\epsilon_{BB}}$ [27], where

$$\chi_{\rm London} = \frac{2\sqrt{I_A I_B}}{I_A + I_B}\left[\frac{2\sqrt{\sigma_{AA}\sigma_{BB}}}{\sigma_{AA}+\sigma_{BB}}\right]^6, \qquad (2)$$

$\sigma_{ij} = (\sigma_i + \sigma_j)/2$ is the average diameter of atoms i and j, and I_A and I_B are the ionization energies of atoms A and B. In Fig. 1 (b), we show the ratio of $\chi_{\rm exp} = \epsilon_{AB}/\sqrt{\epsilon_{AA}\epsilon_{BB}}$ for the experimental data to $\chi_{\rm London}$. More than 70% of the data obeys the London mixing rule with $1 < \chi_{\rm exp}/\chi_{\rm London} < 1.25$. To more fully understand the effects of energetic frustration on the GFA of binary mixtures, below we independently vary $\epsilon_{AB}/\epsilon_{AA}$ and $\epsilon_{BB}/\epsilon_{AA}$ over a much wider range than in Fig. 1 (a).

To quantify the GFA, we analyze the positional order of the system by measuring the bond orientational order parameter for atom i [28, 29]:

$$Q_6(i) = \left[\frac{4\pi}{13}\sum_{m=-6}^{m=6}\left|\frac{1}{N_i+1}\left(q_{6m}(i) + \sum_{j=1}^{N_i} q_{6m}(j)\right)\right|^2\right]^{1/2}, \qquad (3)$$

where $q_{6m}(i) = N_i^{-1}\sum_{j=1}^{N_i}(A_j^i/A_{\rm tot}^i)Y_{6m}(\theta(\boldsymbol{r}_{ij}),\phi(\boldsymbol{r}_{ij}))$, $Y_{6m}(\theta(\boldsymbol{r}_{ij}),\phi(\boldsymbol{r}_{ij}))$ is the spherical harmonic of degree 6 and order m, θ is the polar angle and ϕ is the azimuthal angle of the vector $\boldsymbol{r}_{ij}$ from atom i to j, N_i is the number of Voronoi neighbors of atom i, A_j^i is the area of the Voronoi cell face separating atoms i and j, and $A_{\rm tot}^i$ is the total area of all faces of the Voronoi cell for atom i [29].

The bond orientational order can distinguish between disordered systems ($Q_6 \lesssim 0.3$) and systems with crystalline order [e.g. face-centered cubic (FCC) with $Q_6 = 0.575$, body-centered cubic (BCC) with $Q_6 = 0.511$, and hexagonal close packed (HCP) $Q_6 = 0.485$]. In Fig. 2 (a), we show the fraction f of each sample with local FCC, HCP, BCC, and disordered structure (using adaptive common neighbor analysis [30]) in systems with $f_B = 0.5$ over the full range of cohesive and interaction energies for $R = 5 \times 10^{-5}$. For more than 80% of the systems, the fraction of atoms with FCC or HCP order exceeds 0.70, whereas very few atoms possess BCC order. (We verify this result for other cooling rates in Supplemental Material.) In Fig. 2 (b), we plot the distribution $P(Q_6(i))$ for a system with $\epsilon_{BB}/\epsilon_{AA} = \epsilon_{AB}/\epsilon_{AA} = 1$ and several R. For $R > R_c$, the systems are disordered and $P(Q_6(i))$ has a peak near $Q_6 \approx 0.2$. For $R < R_c$, $P(Q_6(i))$ develops peaks near the values corresponding to FCC and HCP order. The peak near $Q_6(i) \approx 0.535$ corresponds to regions of adjacent FCC and HCP order, not to BCC order as shown in Supplemental Material. In Fig. 2 (c), we show that $\langle Q_6\rangle = N^{-1}\sum_{i=1}^{N} Q_6(i)$ versus R is similar to a logistic function, and R_c can be determined by $R_c = (\langle Q_6\rangle_0 + \langle Q_6\rangle_\infty)/2$, where $\langle Q_6\rangle_0$ and $\langle Q_6\rangle_\infty$ are the values in the limits $R \to 0$ and ∞ limits.

What combination of ϵ_{AA}, ϵ_{BB}, ϵ_{AB}, and f_B controls the GFA in alloys? One possibility is the heat of mixing, which can be generalized for multi-component alloys as $\Delta H_{\rm mix} = 4\sum_{i\neq j} f_i f_j \Delta H_p(i,j)$ [24]. In Fig. 3 (a), we show R_c versus $\Delta H_{\rm mix}$ (normalized by the average cohesive energy $\bar{\epsilon}$) for all binary LJ systems studied. We find little correlation between R_c and $\Delta H_{\rm mix}$ in the simula-

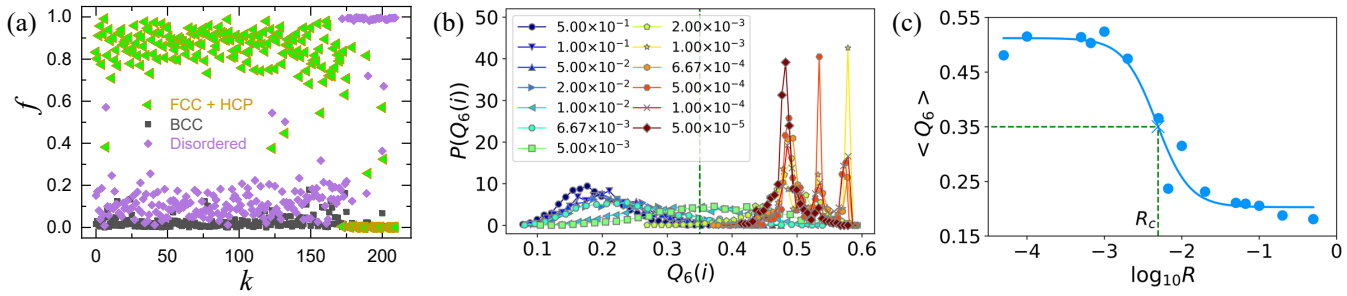

FIG. 2. (a) Fraction f of each system (labelled $k = 1, \ldots, 210$) with a given local structure (FCC, HCP, BCC, or disordered) for a slow cooling rate ($R = 5 \times 10^{-5}$) in binary LJ systems with $f_B = 0.5$ over the full range of cohesive and interaction energies. (b) Distribution of the local bond orientational order parameter $P(Q_6(i))$ for systems with $\epsilon_{BB}/\epsilon_{AA} = \epsilon_{AB}/\epsilon_{AA} = 1.0$ over four orders of magnitude in cooling rate R. (c) Average bond orientational order $\langle Q_6 \rangle$ for the system in (b) versus R. $R_c = (\langle Q_6 \rangle_0 + \langle Q_6 \rangle_\infty)/2$ is obtained by fitting the data to a logistic function $(\langle Q_6 \rangle - \langle Q_6 \rangle_\infty)/(\langle Q_6 \rangle_0 - \langle Q_6 \rangle_\infty) = (1 - \tanh[\log_{10}(R/R_c)^{1/\kappa}])/2$, where $\langle Q_6 \rangle_0$ and $\langle Q_6 \rangle_\infty$ are the average bond orientational order in the limits of $R \to 0$ and ∞, and $0 < \kappa < 1$ is the stretching factor. The vertical dashed line in (b) indicates the $\langle Q_6 \rangle$ that determines R_c (vertical dashed line in (c)).

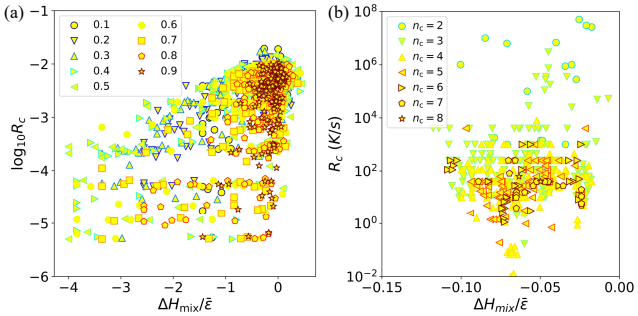

FIG. 3. (a) R_c from simulations of binary LJ systems versus the heat of mixing $\Delta H_{\rm mix}/\bar{\epsilon}$, where $\bar{\epsilon}$ is the average cohesive energy, for nine values of f_B. (b) R_c (in K/s) versus $\Delta H_{\rm mix}/\bar{\epsilon}$ from experiments on 482 metallic glass formers with $n = 2,\ldots,8$ different atomic species.

tions [31]. We also assembled a database of 482 metallic glass formers with $n_c = 2, \ldots, 8$ different atomic species (see Supplemental Material). The experimental data is similar to the simulation data; there is no correlation between R_c and $\Delta H_{\rm mix}$, other than $\Delta H_{\rm mix} < 0$ for all metallic glasses. Note that the simulations cover a much wider range of $\Delta H_{\rm mix}/\bar{\epsilon}$ than experiments on metallic glasses, but R_c in the simulations corresponds to only rapid cooling, 10^{13} to 10^9 K/s.

In Fig. 4 (a) and (b), we show contour plots of R_c versus $\bar{\epsilon}_{AB} = 2\epsilon_{AB}/(\epsilon_{AA} + \epsilon_{BB})$ and $\epsilon_- = (\epsilon_{BB} - \epsilon_{AA})/(\epsilon_{AA} + \epsilon_{BB})$ for binary LJ systems with $f_B = 0.1$ and 0.9. We find strong correlations between R_c and ϵ_- and $\bar{\epsilon}_{AB}$. However, the contours of equal values of R_c in the ϵ_- and $\bar{\epsilon}_{AB}$ plane are very different for $f_B = 0.1$ and 0.9. R_c increases with increasing $\bar{\epsilon}_{AB}$ and increasing ϵ_- for $f_B = 0.1$, whereas R_c increases with increasing $\bar{\epsilon}_{AB}$ and *decreasing* ϵ_- for $f_B = 0.9$. For $f_B \gg f_A$ with a majority of B atoms and only a small fraction of A atoms, to have good GFA, the cohesive interaction between B atoms must be small compared to that for A atoms with $\epsilon_{BB} - \epsilon_{AA} < 0$ and the interaction between A and B atoms must be strong with $\bar{\epsilon}_{AB} \gg 1$. Similarly, when $f_A \gg f_B$ with a majority of A atoms and only a small fraction of B atoms, to have good GFA, the cohesive interaction between B atoms must be strong (or at least comparable to that between A atoms with $\epsilon_{BB} \approx \epsilon_{AA}$) and the interaction between A and B atoms must be strong with $\bar{\epsilon}_{AB} \gg 1$. Note that the R_c contours are symmetric with respect to switching the labels of atoms A and B, and thus we only show the region $\epsilon_{BB} - \epsilon_{AA} \leq 0$.

We approximate the R_c contours as straight lines in the ϵ_- and $\bar{\epsilon}_{AB}$ plane for each f_B and plot the slope k versus f_B in Fig. 4 (c). The slope crosses zero near $f_B \approx 0.2$ and reaches a peak value of $k \approx 0.25$ near $f_B \approx 0.8$. As $f_B \to 1$, the system becomes monoatomic with all B atoms, the GFA depends only on ϵ_-, and thus $k \to 0$. As $f_B \to 0$, the system becomes monoatomic with all A atoms, and the GFA is independent of ϵ_- and $\bar{\epsilon}_{AB}$. In this regime, the slope of the contours in the ϵ_- and $\bar{\epsilon}_{AB}$ plane is undefined as indicated by the vertical dashed line in Fig. 4 (c). In Fig. 4 (d), we show that the data for R_c can be collapsed by plotting $\log_{10} R_c$ versus $[\epsilon_- - k(f_B)\bar{\epsilon}_{AB}]$. We find that the GFA in binary LJ systems obeys a roughly parabolic form:

$$\log_{10} R_c \approx c_1[\epsilon_- - k(f_B)\bar{\epsilon}_{AB}]^2 + \log_{10} R_0, \qquad (4)$$

where $c_1 \approx -2$ gives the concavity and $R_0 \approx 10^{-2}$ is the cooling rate in the $\epsilon_- \to 0$ and $\bar{\epsilon}_{AB} \to 0$ limits.

There are two striking features about the R_c contours in Fig. 4 (a) and (b). First, R_c increases with increasing ϵ_- and $\bar{\epsilon}_{AB}$ for small f_B, indicating that systems with the best GFA possess $\epsilon_{BB} \sim \epsilon_{AA}$ and $\bar{\epsilon}_{AB} \gg 1$. To frustrate crystallization for small f_B, $\epsilon_{BB}/\epsilon_{AA}$ should be

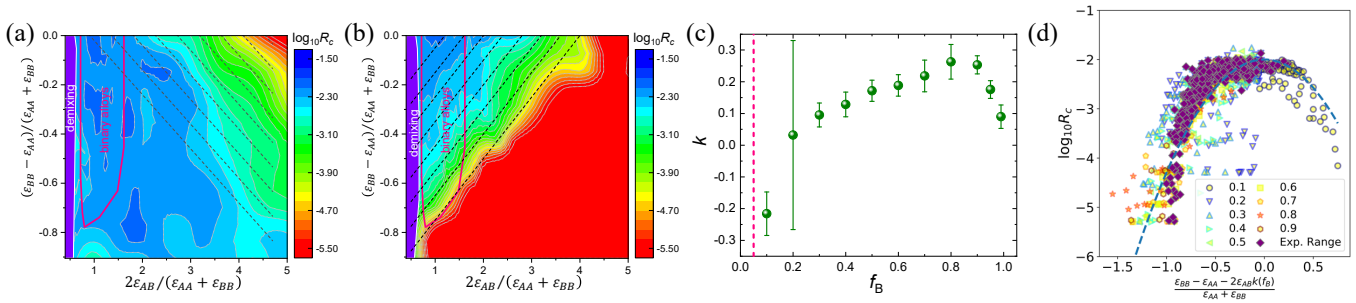

FIG. 4. Contour plots of equal values of R_c (on a logarithmic scale decreasing from blue to red) versus $\bar{\epsilon}_{AB} = 2\epsilon_{AB}/(\epsilon_{AA}+\epsilon_{BB})$ and $\epsilon_- = (\epsilon_{BB}-\epsilon_{AA})/(\epsilon_{AA}+\epsilon_{BB})$ at (a) $f_B = 0.1$ and (b) 0.9. Demixing occurs for $\epsilon_{AB} < (\epsilon_{AA}+\epsilon_{BB})/2$ (purple region). The domain of experimentally accessible binary alloys is enclosed within the solid pink curve (*cf.* Fig. 1 (a)). The dashed lines represent linear approximations of the equal-R_c contours. (c) The best fit slope k of the equal-R_c contour lines in the ϵ_- and $\bar{\epsilon}_{AB}$ plane plotted versus f_B. For $f_B < 0.05$ (vertical dotted line), R_c is uniform and k is undefined. (d) $\log_{10} R_c$ versus $\epsilon_- - k(f_B)\bar{\epsilon}_{AB}$ for all systems studied. The dashed line obeys Eq. 4. Binary LJ systems with ϵ_- and $\bar{\epsilon}_{AB}$ in the experimental range in Fig. 1 (a) are indicated by filled diamonds.

as large as possible, approaching $\epsilon_{BB}/\epsilon_{AA} \to 1$. Similarly, large $\bar{\epsilon}_{AB}$ allows the B atoms to act as low mobility defects with root-mean-square (rms) fluctuations $\Delta r_{AB} = \langle r_{AB}^2\rangle - \langle r_{AB}\rangle^2 < \Delta r_{AA}$ in the low-temperature glass, where $\langle r_{AB}\rangle$ is the average separation between an A atom and a Voronoi-neighbor B atom. (See the Supplemental Material.) Second, R_c increases with decreasing ϵ_- and increasing $\bar{\epsilon}_{AB}$ for large f_B. In this case, $\epsilon_{BB} \to 0$ prevents B atoms from clustering. Also, in the large $\bar{\epsilon}_{AB}$ limit, the A atoms act as low mobility defects with rms fluctuations $\Delta r_{AB} < \Delta r_{BB}$ in the low-temperature glass.

In the high-temperature liquid, the identities of the nearest (Voronoi) neighbors of atoms A and B are completely random. As the system cools, the identities of the neighboring atoms for each atom type A and B can deviate from random, and such chemical ordering can affect the GFA. For example, we hypothesize that if the competing crystal has large chemical order, the system will possess large GFA since the A and B species must rearrange significantly to form the crystal. To assess this hypothesis, we measured the chemical ordering (i.e. the probability $p_A(N_B)$ for an A atom to have N_B B nearest neighbors when $f_A > f_B$ or the probability $p_B(N_A)$ for a B atom to have N_A A nearest neighbors when $f_B > f_A$) at a slow cooling rate with signficant FCC order. In Fig. 5, we show $p_B(N_A)$ for systems with $f_B = 0.9$ and R_c decreasing from (a) to (c). We compare $p_B(N_A)$ to $p_B^{\rm random}(N_A)$, where we keep the low-temperature structure of the system and randomly assign the labels of the nearest neighbors. We find that the GFA increases with the chemical order, $\sum_{N_A} |p_B(N_A) - p_B^{\rm random}(N_A)|$, of the competing crystal. We find similar results for systems with $f_B = 0.1$; the GFA increases with the chemical order, $\sum_{N_B} |p_A(N_B) - p_A^{\rm random}(N_B)|$, of the competing crystal. (See Supplemental Material.)

By decoupling geometric and energetic frustration, we have shown that the GFA is not strongly correlated to the heat of mixing, which involves the particular combination of variables, $(\epsilon_{BB}+\epsilon_{AA})/2\epsilon_{AA} - \epsilon_{AB}/\epsilon_{AA}$. Instead, we find that the GFA is strongly correlated with ϵ_- (i.e. the difference in the cohesive energies, not the sum) and $\bar{\epsilon}_{AB}$, and we identified the f_B-dependent combination of ϵ_- and $\bar{\epsilon}_{AB}$ that controls the GFA for binary LJ systems. We emphasize that it was important to study regions of the ϵ_- and $\bar{\epsilon}_{AB}$ parameter space that were beyond the experimental range of metallic glasses to fully understand the GFA. This work will motivate several important future studies. First, we encourage researchers to experimentally characterize the GFA of binary alloys containing nearly monoatomic elements, yet with large energetic frustration. Second, we are now in a position to understand theoretically the GFA of binary LJ systems with both geometric and energetc frustration. For example, it will be interesting to determine how energetic frustration couples to geometric frustration. For example, should element A with larger cohesive energy possess a larger or smaller metallic radius than element B to yield large GFA?

ACKNOWLEDGEMENTS

The authors acknowledge support from NSF MRSEC Grant No. DMR-1119826 (Y.-C.H.) and NSF Grant Nos. CMMI-1462439 (C.O.) and CMMI-1463455 (M.S.). This work was supported by the High Performance Computing facilities operated by, and the staff of, the Yale Center for Research Computing.

* corey.ohern@yale.edu

[1] J. Schroers, Bulk metallic glasses, Phys. Today **66**, 32 (2013).

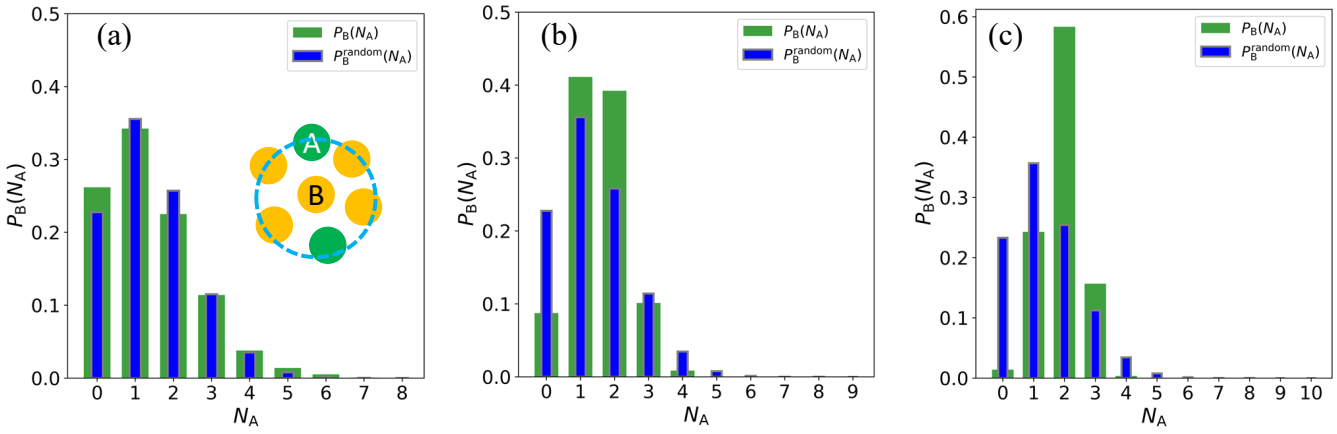

FIG. 5. The probability $P_B(N_A)$ for a B atom to have N_A (Voronoi) nearest neighbors for $f_B = 0.9$ in binary LJ systems cooled at $R = 5 \times 10^{-5}$ (green wide bars) for combinations of ϵ_- and $\bar{\epsilon}_{AB}$ that yield (a) $R_c = 6.6 \times 10^{-4}$ ($\bar{\epsilon}_{AB} = 0.83$, $\epsilon_- = -0.67$), (b) 5.6×10^{-5} ($\bar{\epsilon}_{AB} = 4.17$, $\epsilon_- = -0.11$), and (c) $< 10^{-6}$ ($\bar{\epsilon}_{AB} = 5.0$, $\epsilon_- = -0.67$). We also show $P_B^{\rm random}(N_A)$ (thin blue bars) for systems with the same structure, but randomized atomic labels for the nearest neighbors.

[2] M. D. Demetriou, M. E. Launey, G. Garrett, J. P. Schramm, D. C. Hofmann, W. L. Johnson, and R. O. Ritchie, A damage-tolerant glass, Nat. Mater. **10**, 123 (2011).

[3] W. H. Wang, The elastic properties, elastic models and elastic perspectives of metallic glasses, Prog. Mater. Sci. **57**, 487 (2012).

[4] B. Zberg, P. J. Uggowitzer, and J. F. Löffler, Mgznca glasses without clinically observable hydrogen evolution for biodegradable implants, Nat. Mater. **8**, 887 (2009).

[5] Z. Lu and C. Liu, A new glass-forming ability criterion for bulk metallic glasses, Acta Mater. **50**, 3501 (2002).

[6] A. Inoue, Stabilization of metallic supercooled liquid and bulk amorphous alloys, Acta Mater. **48**, 279 (2000).

[7] D. Xu, B. Lohwongwatana, G. Duan, W. L. Johnson, and C. Garland, Bulk metallic glass formation in binary cu-rich alloy series - $Cu_{100-x}Zr_x$ (x=34, 36, 38.2, 40 at.%) and mechanical properties of bulk $Cu_{64}Zr_{36}$ glass, Acta Mater. **52**, 2621 (2004).

[8] Y. Li, Q. Guo, J. A. Kalb, and C. V. Thompson, Matching glass-forming ability with the density of the amorphous phase, Science **322**, 1816 (2008).

[9] M. B. Tang, D. Q. Zhao, M. X. Pan, and W. H. Wang, Binary Cu-Zr bulk metallic glasses, Chi. Phys. Lett. **21**, 901 (2004).

[10] A.-P. Tsai, A. Inoue, and T. Masumoto, Ductile al-cu-v amorphous alloys without metalloid, Metall. Trans. A **19**, 391 (1988).

[11] L. Zhong, J. Wang, H. Sheng, Z. Zhang, and S. X. Mao, Formation of monatomic metallic glasses through ultrafast liquid quenching, Nature **512**, 177 (2014).

[12] K. Zhang, M. Wang, S. Papanikolaou, Y. Liu, J. Schroers, M. D. Shattuck, and C. S. O'Hern, Computational studies of the glass-forming ability of model bulk metallic glasses, J. Chem. Phys. **139**, 124503 (2013).

[13] H. Shintani and H. Tanaka, Frustration on the way to crystallization in glass, Nat. Phys. **2**, 200 (2006).

[14] D. B. Miracle, A structural model for metallic glasses, Nat. Mater. **3**, 697 (2004).

[15] H. W. Sheng, W. K. Luo, F. M. Alamgir, J. M. Bai, and E. Ma, Atomic packing and short-to-medium-range order in metallic glasses, Nature **439**, 419 (2006).

[16] Y. C. Hu, F. X. Li, M. Z. Li, H. Y. Bai, and W. H. Wang, Five-fold symmetry as indicator of dynamic arrest in metallic glass-forming liquids, Nat. Commun. **6**, 8310 (2015).

[17] Y. Q. Cheng, E. Ma, and H. W. Sheng, Atomic level structure in multicomponent bulk metallic glass, Phys. Rev. Lett. **102**, 245501 (2009).

[18] G. Cargill and F. Spaepen, Description of chemical ordering in amorphous alloys, J. Non-Cryst. Solids **43**, 91 (1981).

[19] S. Nosé, A unified formulation of the constant temperature molecular dynamics methods, J. Chem. Phys. **81**, 511 (1984).

[20] W. G. Hoover, Canonical dynamics: equilibrium phase-space distributions, Phys. Rev. A **31**, 1695 (1985).

[21] G. J. Martyna, D. J. Tobias, and M. L. Klein, Constant pressure molecular dynamics algorithms, J. Chem. Phys. **101**, 4177 (1994).

[22] A. M. Halpern, From dimer to crystal: calculating the cohesive energy of rare gas solids, J. Chem. Educ. **89**, 592 (2012).

[23] A. Takeuchi and A. Inoue, Classification of bulk metallic glasses by atomic size difference, heat of mixing and period of constituent elements and its application to characterization of the main alloying element, Mater. Trans. **46**, 2817 (2005).

[24] A. Takeuchi and A. Inoue, Calculations of mixing enthalpy and mismatch entropy for ternary amorphous alloys, Mater. Trans. **41**, 1372 (2000).

[25] T. Köddermann, D. Paschek, and R. Ludwig, Molecular dynamic simulations of ionic liquids: a reliable description of structure, thermodynamics and dynamics, ChemPhysChem **8**, 2464 (2007).

[26] J. de Andrade, E. S. Böes, and H. Stassen, Computational study of room temperature molten salts composed by 1-alkyl-3-methylimidazolium cations- force-field proposal and validation, J. Phys. Chem. B **106**, 13344

(2002).
[27] F. London, The general theory of molecular forces, Trans. Faraday Soc. **33**, 8 (1937).
[28] P. J. Steinhardt, D. R. Nelson, and M. Ronchetti, Bond-orientational order in liquids and glasses, Phys. Rev. B **28**, 784 (1983).
[29] W. Mickel, S. C. Kapfer, G. E. Schröder-Turk, and K. Mecke, Shortcomings of the bond orientational order parameters for the analysis of disordered particulate matter, J. Chem. Phys. **138**, 044501 (2013).
[30] A. Stukowski, Structure identification methods for atomistic simulations of crystalline materials, Model. Simul. Mater. Sci. Eng **20**, 045021 (2012).
[31] Y. Li, S. Zhao, Y. Liu, P. Gong, and J. Schroers, How many bulk metallic glasses are there?, ACS Comb. Sci. **19**, 687 (2017).